

SPAN-Nav: Generalized Spatial Awareness for Versatile Vision-Language Navigation

Jiahang Liu^{1,2,*} Tianyu Xu^{1,2,*} Jiawei Chen^{1,2,*} Lu Yue^{1,2,*} Jiazhao Zhang^{1,2,*} Zhiyong Wang^{2,*}
Minghan Li² Qisheng Zhao^{1,2} Anqi Li¹ Qi Su^{1,2} Zhizheng Zhang^{2,3,†} He Wang^{1,2,3,†}
¹Peking University ²Galbot ³BAAI

* Equal contribution † Corresponding authors

Project Page: <https://pku-epic.github.io/SPAN-Nav-Web/>

Abstract—Recent embodied navigation approaches leveraging Vision-Language Models (VLMs) demonstrate strong generalization in versatile Vision-Language Navigation (VLN). However, reliable path planning in complex environments remains challenging due to insufficient spatial awareness. In this work, we introduce SPAN-Nav, an end-to-end foundation model designed to infuse embodied navigation with universal 3D spatial awareness using RGB video streams. SPAN-Nav extracts spatial priors across diverse scenes through an occupancy prediction task on extensive indoor and outdoor environments. To mitigate the computational burden, we introduce a compact representation for spatial priors, finding that a single token is sufficient to encapsulate the coarse-grained cues essential for navigation tasks. Furthermore, inspired by the Chain-of-Thought (CoT) mechanism, SPAN-Nav utilizes this single spatial token to explicitly inject spatial cues into action reasoning through an end-to-end framework. Leveraging multi-task co-training, SPAN-Nav captures task-adaptive cues from generalized spatial priors, enabling robust spatial awareness to generalize even to the task lacking explicit spatial supervision. To support comprehensive spatial learning, we present a massive dataset of 4.2 million occupancy annotations that covers both indoor and outdoor scenes across multi-type navigation tasks. SPAN-Nav achieves state-of-the-art performance across three benchmarks spanning diverse scenarios and varied navigation tasks. Finally, real-world experiments validate the robust generalization and practical reliability of our approach across complex physical scenarios.

I. INTRODUCTION

Versatile Vision-Language Navigation (VLN) stands as a cornerstone of embodied intelligence, challenging agents to ground natural language instructions into precise actions within physical environments [1, 2, 3]. While recent efforts have leveraged the potent cross-modal alignment of Vision-Language Models (VLMs) to achieve remarkable generalization [1, 4, 5, 2, 3, 6], their navigational performance often falters when confronting spatially intricate environments, where the reliance on 2D vision observations is insufficient to resolve structural ambiguities, compromising precise localization and jeopardizing safety assurance.

3D spatial awareness is fundamental to reliable navigation, underpinning both high-level spatial grounding and low-level collision avoidance [7, 8, 9]. However, while depth or LiDAR modalities provide such awareness [10, 11], they are physically constrained to visible surface geometry, leaving

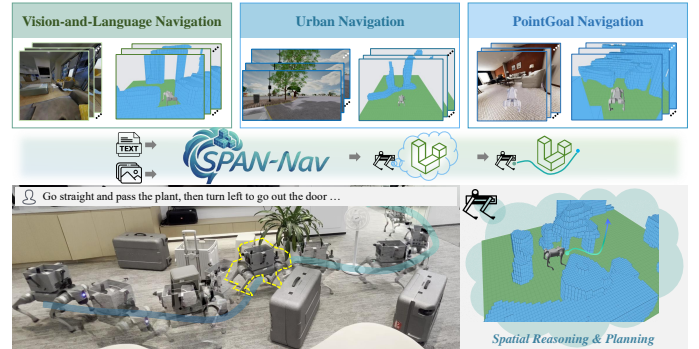


Fig. 1: SPAN-Nav empowers end-to-end embodied navigation with generalized 3D perception. By introducing a Spatially-aware Chain-of-Thought (CoT) mechanism, SPAN-Nav achieves precise and safe navigation in complex environments.

significant blind zones due to occlusion. This partial observability restricts the agent’s amodal completion capabilities, resulting in myopic navigation planning. To address this, 3D occupancy is widely utilized to provide a holistic volumetric representation [12, 13, 14, 15, 16, 17, 18, 19]. Since obtaining ground-truth occupancy necessitates costly environmental scanning and reconstruction, predicting occupancy from RGB inputs has emerged as a more scalable and efficient alternative for perceiving 3D structures. Mainstream occupancy prediction commonly employs Vector Quantized-Variational AutoEncoders (VQ-VAE) [20] to compress continuous 3D scenes into discrete latent representations [12, 13, 14, 16, 19]. While such paradigms thrive in the canonical, regularized environments of autonomous driving, their efficacy diminishes in embodied navigation, where agents confront arbitrary, clutter-filled layouts lacking consistent spatial priors. Consequently, achieving effective and robust spatial awareness across diverse scenes for versatile VLN remains a significant open challenge.

In this work, we present SPAN-Nav, an end-to-end framework that leverages RGB video to facilitate generalized 3D spatial awareness for embodied navigation. To achieve this, we employ continuous latent embeddings that flexibly accommodate the vast scene-structural variability. This approach effectively circumvents the quantization errors and information loss inherent in existing methods, which constrain heterogeneous scenes to a fixed set of discrete priors. Furthermore, to

minimize computational overhead for real-time inference, we condense these continuous embeddings into a single, compact spatial token, facilitating streamlined integration with VLMs. To efficiently leverage the spatial token for action guidance, we employ a Spatial Chain-of-Thought (CoT) mechanism that explicitly grounds decision-making in spatial reasoning. Under extensive cross-task training, this explicit reasoning drives the spatial token to suppress irrelevant volumetric noise and prioritize essential task-relevant cues. Collectively, these innovations endow SPAN-Nav with generalized spatial awareness, ensuring robust navigation across heterogeneous complex environments as shown in Figure 1.

We curated a massive dataset consisting of 4.2 million occupancy annotations, collected from a diverse range of indoor and outdoor environments. The dataset spans both real-world and simulated scenes [21, 22, 23], covering a variety of navigation tasks, including Vision-and-Language Navigation (VLN) [3, 2, 1], urban navigation [24], and collision-free point goal navigation [5]. This diverse exposure enables SPAN-Nav to acquire universal spatial awareness, generalizing robustly across heterogeneous scenes and tasks.

Extensive experiments demonstrate that SPAN-Nav establishes a state-of-the-art (SOTA) across diverse benchmarks, ranging from high-level instruction following to low-level obstacle avoidance in both indoor and outdoor settings. Specifically, on VLN-RxR [25], SPAN-Nav improves the Success Rate (SR) by **5.3%**; on MetaUrban [22], it achieves a **4×** reduction in cumulative cost; and on InternScenes [26] home environments, it yields a **30.9%** higher SR. Beyond standard metrics, SPAN-Nav exhibits remarkable perceptual transfer, generating plausible occupancy maps even on datasets lacking explicit 3D supervision. Real-world deployment further validates this robustness, showing high task completion rates and effective obstacle avoidance in complex, cluttered scenarios.

II. RELATED WORKS

Embodied Navigation Methods. Embodied navigation has witnessed rapid progress in recent years, driven by advances in both modeling approaches and supporting platforms. In particular, the development of simulators [22, 27, 28] and benchmarks [6, 22, 25, 29, 30, 31] has provided standardized tasks and evaluation settings to support scalable training and systematic comparison. Building on these platforms, early approaches [32, 33, 34, 35, 36, 37, 38, 39] employ off-the-shelf large language models (LLMs) with chain-of-thought or structured reasoning, though converting dense visual observations into language often yields sparse and static representations. More recent methods [2, 3, 4, 40, 41, 42, 43, 44] fine-tune image- or video-based vision-language models (VLMs) end-to-end on navigation data, allowing tighter visual–action coupling. Cross-task navigation [1, 2, 45, 46, 47, 48, 49, 50, 51] further demonstrates that jointly learning from versatile navigation tasks improves generalization across scenarios. Nevertheless, performance often falters in spatially intricate environments due to the absence of explicit spatial awareness.

Occupancy Prediction. 3D occupancy has gained increasing attention for its compact and versatile representation of environments, explicitly modeling the occupancy status of each voxel in a 3D grid. MonoScene [52] introduced the first framework for direct prediction of 3D occupancy from monocular images, inspiring subsequent methods [53, 54, 55, 56, 57] that leverage multi-view or depth inputs and voxel-based discretization to efficiently structure 3D scenes and support downstream tasks. More recently, several works [12, 13, 16] have explored occupancy-based world models to enhance spatial perception, and others [14, 18, 19] have integrated occupancy with large language models (LLMs) to predict future 3D occupancy and actions. While these works enable joint learning of 3D occupancy and actions, extending discretized occupancy representations to multi-task and cross-scene navigation remains highly challenging due to limited generalization across diverse tasks and environments.

Chain-of-Thought Reasoning for Embodied AI. Chain-of-Thought (CoT) reasoning has been introduced to embodied AI to bridge high-level semantic understanding and low-level action execution, enabling long-horizon decision making in complex environments. Prior works incorporate CoT into vision-language-action pipelines for navigation [37, 49, 58, 59] and manipulation [60], typically adopting multi-stage training that combines supervised fine-tuning on CoT-annotated trajectories with reinforcement-based optimization. While these approaches improve interpretability and generalization by encouraging reasoning before action, CoT is often expressed in linguistic forms, offering limited support for explicit spatial reasoning and structured environment modeling.

III. OVERVIEW

Task Definition. We formulate embodied navigation as a sequential decision-making process. Given a natural language instruction \mathbf{L} , the agent receives a sequence of RGB observations $\mathbf{V}_t = \{\mathbf{v}_k\}_{k=1}^t$, where \mathbf{v}_k denotes the multi-view RGB inputs at step k . Conditioned on \mathbf{L} and \mathbf{V}_t , the agent predicts a local trajectory $\mathbf{T}_t = \{\mathbf{a}_{t,m}\}_{m=1}^M$ over a planning horizon M . Each predicted pose $\mathbf{a}_{t,m} = (x, y, \theta) \in \mathbb{R}^3$ specifies a target displacement (x, y) and a heading change θ within the agent’s egocentric coordinate system.

Pipeline Overview. SPAN-Nav extends the Qwen3-VL [61] architecture. The pipeline begins by encoding instructions \mathbf{L} into language features \mathbf{E}^L following standard protocols [62]. In Section IV-A, RGB inputs \mathbf{V}_t are processed via the vision encoder and cross-modal projector of Qwen3-VL, incorporating a spatiotemporal compression strategy [1] to yield efficient visual representations \mathbf{E}_t^V . Subsequently, to learn a compact and generalized spatial token, \mathbf{E}_t^V and \mathbf{E}^L flow into the VLM backbone and output a compact spatial token through a cross-scene occupancy prediction supervision in Section IV-B. This token then serves as a spatial prior and is explicitly injected into the action reasoning process via a CoT mechanism in Section IV-C, ultimately generating the spatially-aware trajectory. Finally, Section IV-D details our training strategy, which

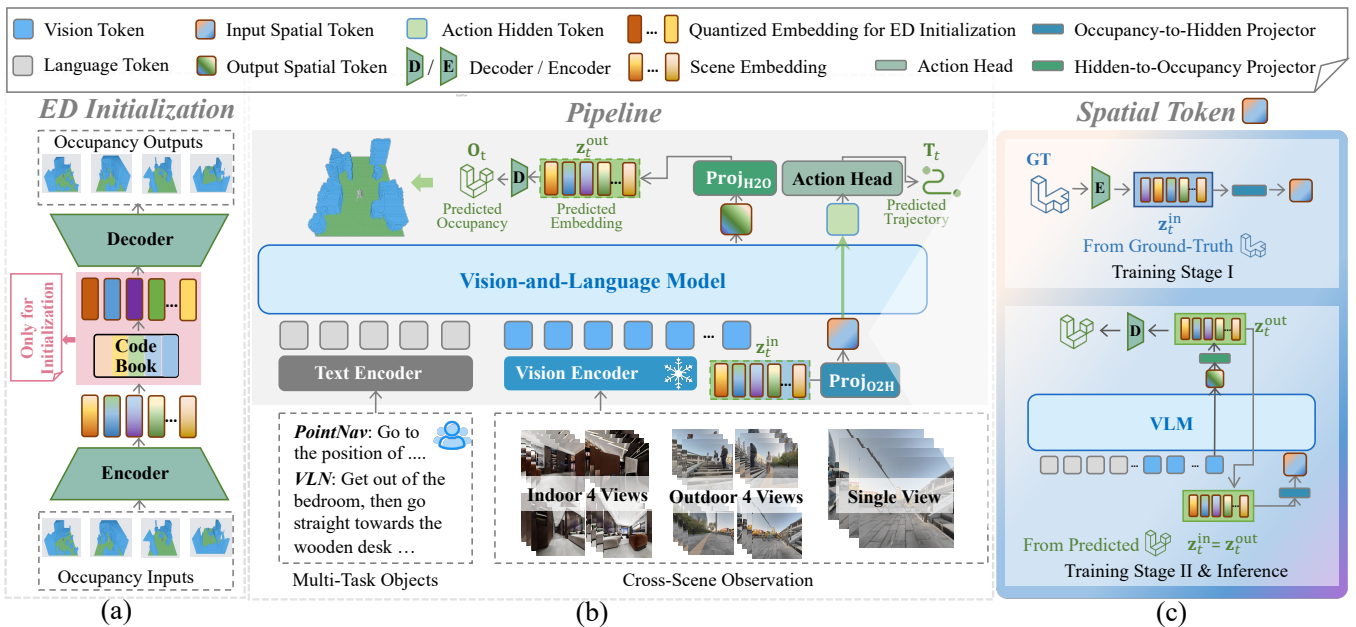


Fig. 2: **Overview of SPAN-Nav.** (a) Encoder-Decoder (ED) Initialization. We pre-train a VQ-VAE-based architecture on cross-scene occupancy datasets. This initializes the perceptual representation capabilities of the encoder and decoder, facilitating subsequent end-to-end training. (b) SPAN-Nav Pipeline. SPAN-Nav leverages a VLM-based architecture to learn 3D spatial awareness through a designed spatial token, which is explicitly injected into the navigation reasoning process, facilitating efficient and spatially-aware decision-making. (c) Adaptive Spatial Token Acquisition. The source of the spatial token adapts to the training phase. In training stage I, tokens are derived from Ground-Truth (GT) occupancy. In training stage II and during inference, the model switches to relying on its self-predicted spatial tokens.

coordinates these components to achieve robust navigation grounded in generalized perception.

IV. MODEL OF SPAN-NAV

A. Observation Encoding

Here, we detail the pipeline for processing RGB observations. The vision encoder from Qwen3-VL [61] is employed to extract visual features from the observation sequence \mathbf{V}_t . Since continuous navigation generates an excessive volume of frames and features, we implement a spatiotemporal compression strategy [1] to manage this redundancy. Specifically, we first downsample the history frame number to a fixed count via a probabilistic sampling function. Then, we apply average pooling to the sampled history features for spatial aggregation. Finally, these compressed historical features are concatenated with the intact features of the current frame and projected into the latent space to serve as the final visual input \mathbf{E}_t^V .

B. Cross-Scene Spatial Token Learning

To achieve reliable spatial awareness across diverse environments, we introduce a compact, generalized spatial representation learned from an occupancy prediction task and align it with the internal representations of VLM to efficiently achieve cross-scene representations.

Encoder-Decoder Initialization. As shown in Figure 2 (a), inspired by state-of-the-art occupancy prediction methods in autonomous driving [12, 13, 14, 16, 19], we employ a scene tokenizer based on Vector-Quantized Variational Autoencoder (VQ-VAE) [20], pre-trained on our large-scale annotated occupancy dataset, to initialize the occupancy encoder and

decoder. This strategy incorporates 3D spatial priors to facilitate efficient downstream end-to-end training. We represent the ego-centric 3D environment as a binary occupancy map $\mathbf{O}_t \in \{0, 1\}^{H \times W \times D}$, where voxels are labeled 0 for free space and 1 for obstacles. Leveraging a VQ-VAE framework, a lightweight encoder $\text{Enc}(\cdot)$ first maps \mathbf{O}_t to continuous occupancy latent embeddings \mathbf{z}_t . Then, \mathbf{z}_t are subsequently quantized into discrete representations $\hat{\mathbf{z}}_t$ via nearest-neighbor retrieval from a learnable codebook. Finally, a decoder $\text{Dec}(\cdot)$ reconstructs the occupancy \mathbf{O}_t from $\hat{\mathbf{z}}_t$, which is further optimized via a supervisory loss relative to the ground truth \mathbf{O}_t^{GT} . Through training this framework on massive occupancy-annotated datasets covering indoor and outdoor environments, 3D perception priors are injected into $\text{Enc}(\cdot)$ and $\text{Dec}(\cdot)$.

Compact Cross-Scene Spatial Token. To establish a robust spatial representation capable of handling complex cross-domain scenes, we investigated VQ-VAE based approaches and empirically observed that utilizing quantized features yields underwhelming performance for embodied navigation tasks (see Table IV in Section VI). We argue that while discrete quantization in VQ-VAE is highly effective for structured and homogeneous scenes, it struggles to adequately characterize the heterogeneity inherent to highly diverse and unstructured embodied environments. As a result, we discard the use of the discrete quantization and employ continuous occupancy latent embeddings \mathbf{z}_t as a compact spatial representation for VLM integration (Figure 2 (b)-(c)). We introduce two projectors to bidirectionally align \mathbf{z}_t with the VLM's hidden space. First, the projector $\text{Proj}_{O2H}(\cdot)$ maps the input occupancy features \mathbf{z}_t^{in} with dense volumetric features into the VLM's hidden space.

This process compresses the spatial awareness into a single input spatial token \mathbf{h}_t^{in} :

$$\mathbf{h}_t^{\text{in}} = \text{Proj}_{\text{O2H}}(\mathbf{z}_t^{\text{in}}). \quad (1)$$

Conversely, for the generation process, the VLM leverages language embeddings \mathbf{E}_t^{L} and visual embeddings \mathbf{E}_t^{V} to predict an output hidden state $\mathbf{h}_t^{\text{out}}$. The second projector, $\text{Proj}_{\text{H2O}}(\cdot)$, maps this state back to the occupancy embedding space to yield the predicted features $\mathbf{z}_t^{\text{out}}$:

$$\mathbf{h}_t^{\text{out}} = \text{VLM}(\mathbf{E}_t^{\text{L}}, \mathbf{E}_t^{\text{V}}), \quad \mathbf{z}_t^{\text{out}} = \text{Proj}_{\text{H2O}}(\mathbf{h}_t^{\text{out}}). \quad (2)$$

This representation strategy requires the model to distill salient spatial cues into a concise representation without incurring significant computational overhead. Notably, the spatial token is sourced from either ground-truth or self-predicted occupancy, depending on the corresponding training stage (Section IV-D).

Cross-Scene Occupancy Supervision. For the cross-scene occupancy prediction task, we designed two spatially-aware optimization objectives, aimed at fostering interpretable perceptual capabilities for SPAN-Nav. Specifically, we first utilize SPAN-Nav’s VLM framework to predict $\mathbf{z}_t^{\text{out}}$ and $\mathbf{h}_t^{\text{out}}$ as illustrated in Equation (2). $\mathbf{z}_t^{\text{out}}$ is then processed by the initialized decoder to reconstruct an occupancy grid:

$$\mathbf{O}_t = \text{Dec}(\mathbf{z}_t^{\text{out}}). \quad (3)$$

The predicted occupancy is supervised by calculating the reconstruction loss against the ground truth:

$$\mathcal{L}_{\text{occ}} = \mathcal{L}_c(\mathbf{O}_t^{\text{GT}}, \mathbf{O}_t) + \mathcal{L}_l(\mathbf{O}_t^{\text{GT}}, \mathbf{O}_t), \quad (4)$$

where \mathbf{O}_t^{GT} is the ground-truth occupancy. $\mathcal{L}_c(\cdot)$ represents the cross-entropy loss and $\mathcal{L}_l(\cdot)$ represents the Lovász-softmax loss (see Section VIII for details). This supervision enables the model to effectively abstract 3D scene features conducive to local environmental reconstruction directly from 2D observations. Furthermore, to ensure a high-fidelity representation, we impose explicit supervision on $\mathbf{z}_t^{\text{out}}$:

$$\mathcal{L}_{\text{latent}} = \|\text{Enc}(\mathbf{O}_t^{\text{GT}}) - \mathbf{z}_t^{\text{out}}\|_2^2. \quad (5)$$

Collectively, these two supervision signals ensure that SPAN-Nav not only reconstructs accurate 3D geometry but also preserves a latent manifold throughout the reasoning process.

C. Spatial Chain-of-Thought Action Reasoning

To better integrate the extracted spatial information with action generation, we do not treat spatial information prediction as a simple auxiliary task. Instead, we explicitly incorporate it as part of the Chain-of-Thought (CoT) reasoning process to assist action planning. This spatial-aware CoT strategy decomposes navigation into a sequential ‘perception-then-action’ inference process, transitioning action generation from a heuristic mapping to a grounded decision-making framework rooted in explicit 3D environmental understanding derived from $\mathbf{z}_t^{\text{out}}$ (obtained via Equation (2)). The generation process of the predicted trajectory \mathbf{T}_t is formalized as follows,

$$\mathbf{E}_t^{\text{act}} = \text{VLM}(\mathbf{E}_t^{\text{L}}, \mathbf{E}_t^{\text{V}}, \text{Proj}_{\text{O2H}}(\mathbf{z}_t^{\text{out}})), \quad \mathbf{T}_t = \text{AH}(\mathbf{E}_t^{\text{act}}), \quad (6)$$

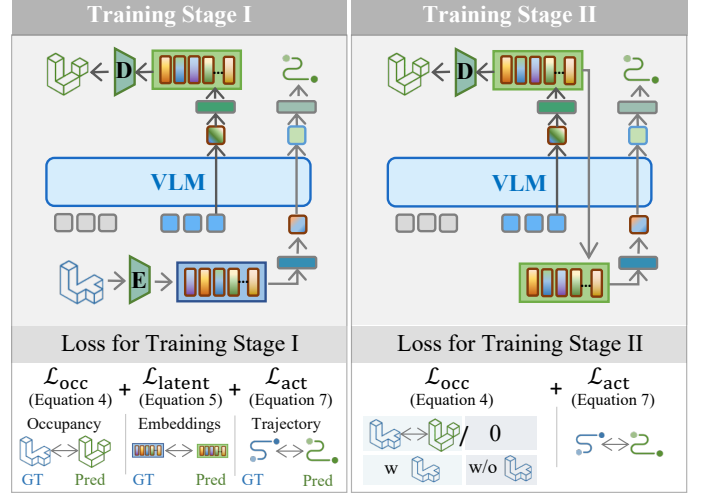


Fig. 3: **Training stages for navigation-specific tasks.** In Stage I, SPAN-Nav is trained via teacher-forcing using ground-truth (GT) occupancy, jointly supervised by occupancy, spatial representation and action. Stage II transitions to student-forcing, inferring actions from self-predicted spatial tokens. Notably, \mathcal{L}_{occ} only applies when GT occupancy is available in this stage. (Legends follow Figure 2.)

where $\mathbf{E}_t^{\text{act}}$ represent the predicted action hidden state, and $\text{AH}(\cdot)$ is a multi-layer MLP for trajectory planning. We employ trajectory supervision on massive cross-domain datasets to refine the model by minimizing the following loss function,

$$\mathcal{L}_{\text{act}} = \|\mathbf{T}_t^{\text{GT}} - \mathbf{T}_t\|_2^2, \quad (7)$$

where \mathbf{T}_t^{GT} is the ground-truth trajectory. This process empowers the CoT mechanism to sift through complex 3D data, focusing on navigation-critical cues like traversable paths while ignoring irrelevant volumetric noise.

D. Training Strategy

During training, we employ a co-training strategy that integrates general QA data with navigation-specific data, comprising both 3D occupancy prediction and trajectory reasoning. The loss function for the QA task is defined as \mathcal{L}_{qa} (see Section VIII for details). Regarding navigation tasks, we implement a two-stage training regimen with distinct optimization objectives as shown in Figure 3. In the first stage, we leverage extensive cross-scene and multi-task datasets with full occupancy annotations to train SPAN-Nav with a teacher-forcing mechanism and a joint optimization objective. Specifically, we establish robust 3D spatial awareness and enable SPAN-Nav to reason actions based on noise-free, ground-truth spatial representations. The joint loss for this phase is:

$$\mathcal{L}_{\text{s1}} = \mathcal{L}_{\text{occ}} + \mathcal{L}_{\text{latent}} + \mathcal{L}_{\text{act}} + \mathcal{L}_{\text{qa}}, \quad (8)$$

where \mathcal{L}_{occ} , $\mathcal{L}_{\text{latent}}$, and \mathcal{L}_{act} correspond to occupancy reconstruction, latent consistency, and action supervision losses as formulated in Equations (4), (5) and (7), respectively. Notably, to mitigate the perceptual noise interference, the action reasoning process in Equation (6) is conditioned on latent embeddings extracted directly from the ground-truth occupancy; specifically, we set $\mathbf{z}_t^{\text{out}} = \mathbf{z}_t^{\text{GT-out}}$, where $\mathbf{z}_t^{\text{GT-out}} = \text{Enc}(\mathbf{O}_t^{\text{GT}})$.

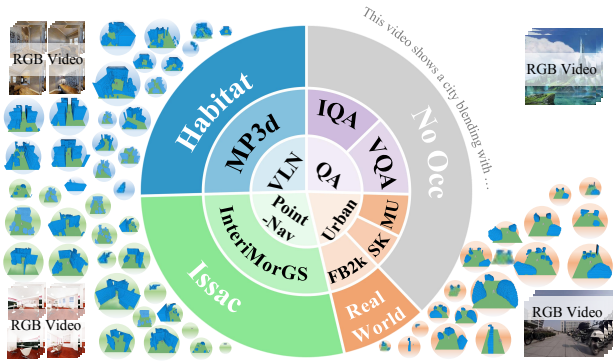


Fig. 4: **Dataset composition and occupancy-map visualization.** Sunburst summary of our data composition. The inner ring groups samples by task, the middle ring by dataset, and the outer ring by occupancy-map (Occ) source / availability. MU, SK, and FB2K denote MetaUrban, SeKai, and FrodoBots-2K, respectively.

Subsequently, in the second stage, we bridge the gap between training and inference by transitioning the trajectory planning process to rely on the model’s self-predicted occupancy latent embeddings (i.e., z_t^{out} obtained via Equation (2)). This stage is conducted on a mixed dataset comprising both occupancy-annotated and unannotated samples. We formulate the optimization objective to balance two goals: maintaining high-fidelity spatial interpretation via the occupancy loss (Equation (4)), and adapting the policy to internal spatial reasoning via the action loss (Equation (7)). The total loss is defined as follows,

$$\mathcal{L}_{s2} = \mathcal{L}_{\text{occ}} + \mathcal{L}_{\text{act}} + \mathcal{L}_{\text{qa}}, \quad (9)$$

where \mathcal{L}_{occ} is set to 0 for samples lacking ground-truth occupancy annotations. This fine-tuning process empowers SPAN-Nav to prioritize navigation-critical spatial features over irrelevant volumetric noise while maintaining grounded spatial awareness, enabling robust end-to-end inference.

V. DATASET OF SPAN-NAV

A. Overview

To train SPAN-Nav, we have carefully constructed a diverse dataset that covers a wide range of indoor and outdoor environments across various navigation tasks. The dataset contains a total of 7.08M data points, including 5.08M trajectory data, 0.93M ImageQA, and 1.07M Video-QA, along with 4.2M occupancy-annotated data points to support spatial awareness understanding. The data sources include both simulated environments and real-world scenarios, ensuring comprehensive coverage of varied settings. The dataset includes three key navigation tasks. **Vision-Language Navigation (VLN)** requires the agent to interpret natural language instructions and align them with visual inputs to reach landmarks, demanding strong instruction-following and visual reasoning. **Urban Navigation** involves navigating urban environments with instructions to a target location, emphasizing path planning and obstacle avoidance in dynamic settings. **PointGoal Navigation** requires reaching a target location based on coordinate-based instructions, focusing on collision avoidance. Each of these tasks

necessitates spatial awareness to understand the environment effectively. Together, they cover the major aspects of navigation, including instruction interpretation, path planning, and safe navigation in cross-scene environments.

B. Navigation Data Collection for Multi Task

All navigation data are collected in a unified manner, including egocentric captured videos (from both single and multiple cameras), instructions, and GT trajectory waypoints. For obtaining GT trajectories, we have designed different data collection methods for each task to ensure accurate and task-specific annotations.

VLN (1.8M): We collect data from VLN-CE’s R2R and RxR tasks by capturing egocentric RGB videos, natural language instructions, and trajectory information as the robot followed the ground-truth path. Additionally, following the approach in [63], we collect an extra round of DAgger data to further enhance the training process. **Urban Navigation (1.28M):** Simulation trajectories are gathered in the MetaUrban simulator, and real-world data are sourced from the Sekai[64] and FrodoBots-2K [65] datasets. To reduce noise and limited observability in the real-world data, we reconstruct smooth 2D trajectories and enhance them with Heuristic Trajectory Lifting (HTL) [24]. **Point Goal Navigation (2M):** We randomly sample start and end points in the InteriorGS dataset [66], which includes 1,000 large-scale indoor scenes. Smooth, collision-free trajectories are then generated using an online A^*+VO fusion planner (see Section VIII for details), and are naturally aligned with our CoT occupancy supervision.

C. Occupancy Annotation

To efficiently collect Occupancy Annotations in bulk, we have developed separate pipelines for simulated and real-world data to ensure fast and accurate labeling.

Annotation in the Simulator. We first convert the 1091 scene datasets (from InteriorGS [67] and MP3D [68]), specifically used in our study, into a format compatible with Isaac Sim [28]. Using Isaac Sim, we extract 3D occupancy information from the scenes, with each occupancy voxel having dimensions of 0.05m in width and length and 0.1m in height. Based on the robot’s position at each moment, we collect surrounding occupancy data covering a 4m range in front, 2m behind, and 2m on either side.

Annotation in the Real World. Occupancy supervision is generated for FrodoBots-2K [65] data. Due to the lack of complete spatial information of the entire scene, we use a feed-forward reconstruction model (Depth Anything 3 [69]) to reconstruct the scene. The reconstructed point clouds are voxelized and labeled as occupied or unoccupied. After that, we apply the same method as in the simulator to label the occupancy map centered around the agent.

VI. EXPERIMENTS

To evaluate the performance of SPAN-Nav, we focus on two key aspects: 1) the model’s performance across multiple benchmarks, including its spatial awareness capabilities, 2)

TABLE I: Comparison on VLN-CE across RGB-Only and Multi-Sensory (RGB-D + Odometry) settings. The symbol * indicates methods utilizing the waypoint predictor from [70]. Remarkably, relying solely on RGB video, our method achieves state-of-the-art performance, surpassing prior works that depend on auxiliary depth and odometry inputs.

Method	Observation			R2R Val-Unseen				RxR Val-Unseen			
	RGB	Depth	Odo.	NE ↓	OS ↑	SR ↑	SPL ↑	NE ↓	SR ↑	SPL ↑	nDTW ↑
CMA* [70]	✓	✓	✓	6.20	52.0	41.0	36.0	8.76	26.5	22.1	47.0
VLN ^o BERT* [70]	✓	✓	✓	5.74	53.0	44.0	39.0	8.98	27.0	22.6	46.7
AO-Planner [71]	✓	✓		5.55	59.0	47.0	33.0	7.06	43.3	30.5	50.1
Reborn* [72]	✓	✓	✓	5.40	57.0	50.0	46.0	5.98	48.6	42.0	63.3
ETPNav* [73]	✓	✓	✓	4.71	65.0	57.0	49.0	5.64	54.7	44.8	61.9
HNR* [74]	✓	✓	✓	4.42	67.0	61.0	51.0	5.50	56.3	46.7	63.5
NaVid [3]	✓			5.72	49.2	41.9	36.5	5.72	45.7	38.2	-
NaVILA [40]	✓			5.22	62.5	54.0	49.0	6.77	49.3	44.0	58.8
Uni-NaVid [2]	✓			5.58	53.3	47.0	42.7	6.24	48.7	40.9	-
Stream VLN [41]	✓			4.98	64.2	56.9	51.9	6.22	52.9	46.0	61.9
NavFom [1]	✓			4.61	72.1	61.7	55.3	4.74	64.4	56.2	65.8
SPAN-Nav Generalize	✓			4.02	73.1	63.3	57.3	4.50	66.5	57.0	67.3
SPAN-Nav	✓			4.07	75.3	66.3	59.3	4.20	69.7	60.1	67.9

the effectiveness of our core design. We conducted extensive experiments on the three tasks mentioned in Section V-A, as well as ablation studies.

A. Experiment Setup

To evaluate our method, we focus on its performance across various navigation tasks and the robustness of its spatial awareness. This section outlines the evaluation benchmarks, performance metrics, and the implementation details.

Benchmarks. We evaluate our method across multiple navigation benchmarks, including VLN, Urban Navigation, and PointGoal Navigation. For VLN, we assess our approach on the Val-UnSeen split of the VLN-CE R2R [29] and RxR [25] benchmarks. In Urban Navigation, we test on MetaUrban’s PointNav and SocialNav benchmarks [22], using 1,000 scenes from MetaUrban-test and 100 unseen scenes, with a wheelchair embodiment for fair comparison with low-level control settings. For PointGoal Navigation, we follow InternVLA-N1 (S1) [6, 10], evaluating on 40 scenes from the InternScenes [26] dataset, with the same 100 start-goal pairs as in InternVLA-N1, and using the Dingo robot platform with omnidirectional control.

Metrics. To evaluate navigation performance, we follow standard evaluation metrics [75], including Success Rate (SR), Oracle Success rate (OS), Success rate weighted by Path Length (SPL), cumulative Cost for collision avoidance (Cost), Social Navigation Score for social compliance (SNS), normalized Dynamic Time Warping (nDTW), and Navigation Error relative to the goal (NE). Note that the success criteria for different navigation tasks may vary; thus, we use the default success criteria defined for each benchmark.

Implementation Details. SPAN-Nav is built upon Qwen3-VL [61] and is trained on the dataset described in Section V. We train the model on 32 NVIDIA H100 GPUs for approximately one day, totaling 768 GPU hours. For real-world deployment, SPAN-Nav runs on a Unitree GO2 quadruped robot equipped with four SG3S11AFxK cameras for multi-view RGB streaming. The video streams are transmitted to a remote server with an NVIDIA RTX 4090 GPU, where SPAN-Nav predicts spatial information and generates trajectory waypoints for execution

on the onboard controller (see Section VIII for details).

B. Benchmark Results

Performance Analysis. We evaluate SPAN-Nav across three tasks: VLN, Urban Navigation, and Point Goal Navigation, using the benchmarks mentioned in Section VI-A. On all these benchmarks, SPAN-Nav achieves state-of-the-art (SOTA) performance. In the VLN task, as shown in Table I, SPAN-Nav outperforms the previous SOTA, NavFoM [1], with a 4.6% improvement in success rate (SR) on R2R and a 5.3% improvement on RxR, despite being trained on fewer data (12.7M vs. 7.08M). For Urban Navigation, on the MetaUrban benchmark, SPAN-Nav shows significant improvements, outperforming multiple prior approaches, including RL methods [76, 77, 78, 79, 80], imitation learning baselines [81, 82], and VLA baselines [24]. As shown in Table II, SPAN-Nav significantly reduces cumulative cost (Cost) by over 4× compared to UrbanVLA, while maintaining near-perfect social compliance (SNS=0.96). In Point Goal Navigation, SPAN-Nav also achieves substantial performance improvements, with a success rate exceeding 30.9% in home environments and 19.6% in commercial environments, as reported in Table III.

Qualitative Analysis. As shown in the visualization results of Figure 5, the success of SPAN-Nav is attributed to its explicit spatial perception, which enables efficient collision avoidance and trajectory planning through reasoning results that guide trajectory generation. SPAN-Nav extracts spatial information and predicts occupancy, enabling amodal completion capabilities for safe navigation in complex environments, while improving path efficiency. To further validate the generalization capability of our spatial awareness, we trained a variant of SPAN-Nav (denoted as SPAN-Nav Generalize), where we removed the VLN occupancy annotations during both stage I and stage II of training. This adjustment aimed to assess whether the model could generalize spatial awareness to the VLN task using the occupancy supervision from the Urban Navigation and Point Goal Navigation tasks. As shown in Table I, despite a slight performance decrease, SPAN-Nav still outperforms previous methods, demonstrating its ability to transfer spatial awareness to VLN tasks.

TABLE II: Comparison on the benchmark of PointNav and SocialNav tasks in the MetaUrban-12K dataset. We compare our method with seven strong baselines with LiDAR observation. The **best** and the second best results are denoted by **bold** and underline, respectively.

Method	Observation	PointNav (Test)			PointNav (Unseen)			SocialNav (Test)			SocialNav (Unseen)		
		SR \uparrow	SPL \uparrow	Cost \downarrow	SR \uparrow	SPL \uparrow	Cost \downarrow	SR \uparrow	SNS \uparrow	Cost \downarrow	SR \uparrow	SNS \uparrow	Cost \downarrow
PPO [76]	LiDAR	66	64	0.51	49	45	0.78	34	64	0.66	24	57	0.51
PPO-Lag [77]	LiDAR	60	58	<u>0.41</u>	60	57	<u>0.53</u>	17	51	0.33	8	47	<u>0.50</u>
PPO-ET [78]	LiDAR	57	53	0.47	53	49	0.65	5	52	<u>0.26</u>	2	50	0.62
IQL [79]	LiDAR	36	33	0.49	30	27	0.63	36	67	0.39	27	62	3.05
TD3+BC [80]	LiDAR	29	28	0.77	20	20	1.16	26	61	0.62	32	64	1.53
BC [81]	LiDAR	36	28	0.83	32	26	1.15	28	56	1.23	18	54	0.58
GAIL [82]	LiDAR	47	36	1.05	40	32	1.46	34	63	0.71	28	61	0.67
UrbanVLA [24]	RGB	94	<u>91</u>	0.94	97	95	0.84	<u>91</u>	<u>87</u>	0.81	88	<u>85</u>	0.82
SPAN-Nav	RGB	94	93	0.22	<u>92</u>	<u>91</u>	0.20	92	96	0.19	93	96	0.28

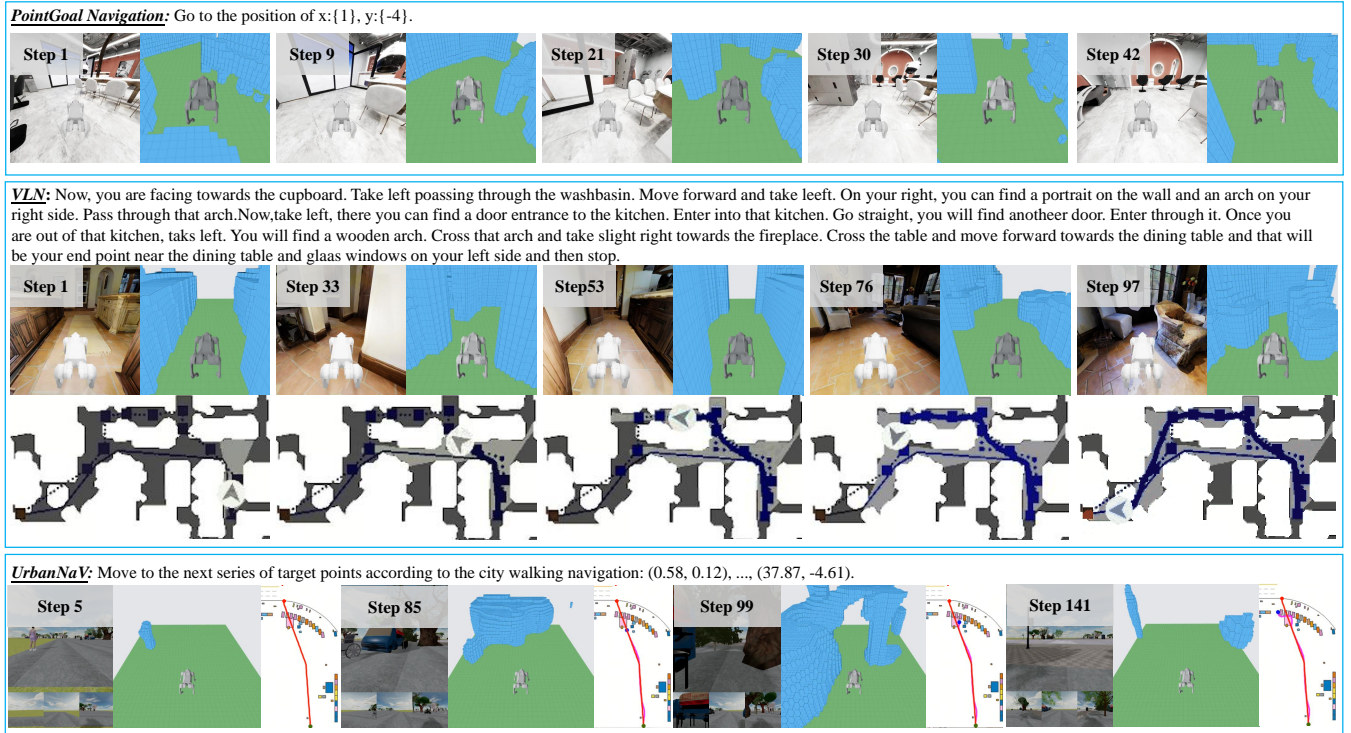


Fig. 5: **Experimental visualization of SPAN-Nav across diverse tasks in different simulators.** This includes PointGoal Navigation, VLN, and UrbanNav, encompassing a variety of complex indoor and outdoor scenarios. Across these tasks, SPAN-Nav consistently plans safe and robust trajectories, ensuring high navigation success rates.



Fig. 6: **Real-world experimental demonstration.** SPAN-Nav demonstrates strong transferability, achieving precise obstacle avoidance and reliable task execution.

C. Real-World Results

We conducted additional real-world experiments to demonstrate the generalization capability of our model in unseen environments. Our experiments were set up according to the configuration outlined in Section VI-A, and the visualiza-

tion results are shown in Figure 6. We present the model’s performance in the presence of transparent glass and its ability to navigate scenarios requiring fine obstacle avoidance, while also visualizing the Occupancy predictions it generates. These results demonstrate the role of spatial awareness in trajectory planning, where the model leverages detailed spatial information to enhance navigation accuracy and make more informed decisions, particularly in complex environments.

D. Ablation Study

Ablation on model architecture. To analyze the contribution of key architectural components, we compare SPAN-Nav with three variants: (i) replacing continuous occupancy representations with discrete VQ-VAE tokens (*Discrete Token*), (ii) removing occupancy supervision (*w/o Occupancy*), and

TABLE III: **Simulation results in InternVLA-N1 System-1 point-goal navigation benchmark.** The symbol \dagger indicates zero-shot evaluation without additional fine-tuning on Interscenes dataset.

Method	Obs.	Home		Commercial	
		SR \uparrow	SPL \uparrow	SR \uparrow	SPL \uparrow
DD-PPO [83] \dagger	RGB-D	0.4	0.4	5.3	5.2
iPlanner [84] \dagger	Depth	43.0	40.6	54.6	52.8
ViPlanner [85] \dagger	RGB-D	45.0	43.2	63.7	61.9
LoGoPlanner [86]	RGB-D	57.3	52.4	67.1	63.9
InternVLA-N1 [6](S1)	RGB-D	60.0	55.6	71.4	68.2
MM-Nav [5] \dagger	RGB	32.2	31.7	61.1	60.8
SPAN-Nav (w/o Occ.) \dagger	RGB	70.5	67.9	75.1	73.1
SPAN-Nav (w/o CoT) \dagger	RGB	81.3	77.2	85.2	82.3
SPAN-Nav\dagger	RGB	90.9	85.7	91.0	88.1

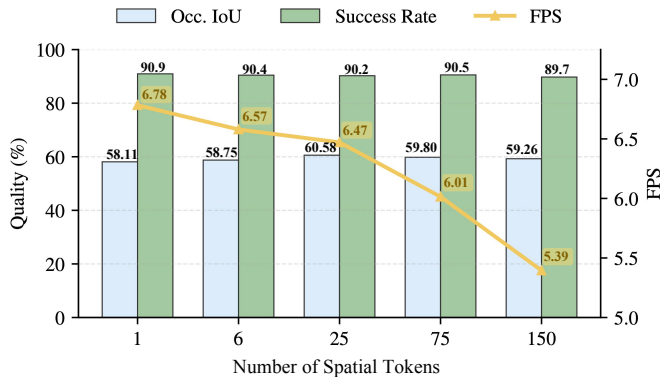


Fig. 7: **Ablation study on the number of spatial tokens used for occupancy reconstruction.** We report occupancy reconstruction quality (IoU), success rate (SR) in point-goal navigation, and inference efficiency (FPS) under different spatial token budgets.

(iii) removing the spatial Chain-of-Thought (CoT) reasoning module (*w/o CoT*). The quantitative results in Table IV show that using discrete VQ-VAE tokens significantly degrades occupancy reconstruction quality, with IoU dropping from 58.11 to 45.03. This suggests that quantized codebook representations struggle to capture diverse spatial layouts in embodied navigation, where strong spatial priors are often absent and discretization will introduce irreversible information loss. Removing occupancy supervision causes a large performance drop, with SR / SPL falling to 70.5 / 67.9 on the Home split and 75.1 / 73.1 on the Commercial split, highlighting its importance for spatial awareness and action planning. Eliminating the spatial CoT reasoning module leads to consistent declines in SR / SPL (Home: 81.3 / 77.2; Commercial: 85.2 / 82.3), showing that explicit spatial reasoning aids action selection. The slight IoU drop of SPAN-Nav compared to *w/o CoT* arises because spatial CoT reasoning prioritizes navigation-critical occupancy cues over fine-grained geometric details; further analysis is provided in the supplementary material. Overall, SPAN-Nav achieves the best performance (Home: 90.9 / 85.7; Commercial: 91.0 / 88.1) while maintaining strong occupancy reconstruction.

Ablation on training strategy. We further investigate two training-related design choices: encoder-decoder (ED) ini-

TABLE IV: **Ablation study on architectural components and training strategies.** All variants are trained on the same data and evaluated in terms of occupancy reconstruction quality (IoU) and point-goal navigation performance (SR/SPL) on the InternVLA-N1 System-1 benchmark.

Setting	IoU($\%$) \uparrow	Home		Commercial	
		SR \uparrow	SPL \uparrow	SR \uparrow	SPL \uparrow
discrete token	45.03	80.3	78.0	80.0	78.4
w/o Occupancy	-	70.5	67.9	75.1	73.1
w/o CoT	60.71	81.3	77.2	85.2	82.3
w/o ED initialization	41.67	85.0	80.7	84.7	82.2
w/o Training Stage II	58.04	56.8	54.7	67.3	66.2
SPAN-Nav	58.11	90.9	85.7	91.0	88.1

tialization (*w/o ED Initialization*) and the two-stage training strategy (*w/o Training stage II*), as summarized in Table IV. Without ED initialization, occupancy reconstruction quality deteriorates substantially (IoU drops to 41.67), accompanied by degraded navigation performance. This underscores the importance of a well-initialized spatial encoder-decoder for stabilizing training and facilitating effective spatial representation learning. More critically, removing stage II causes a pronounced decline in navigation performance (Home: 56.6 / 54.5; Commercial: 68.1 / 66.9), despite similar occupancy IoU (58.04 vs. 58.11). This observation indicates that stage II is essential for aligning the action policy with *self-predicted* spatial tokens during inference, preventing a train-test mismatch that significantly weakens downstream control performance.

Ablation on the number of spatial tokens. To evaluate the effectiveness and efficiency of our compact cross-scene spatial token representation, we further conduct an ablation study by varying the number of spatial tokens used for spatial perception and occupancy reconstruction. The results are summarized in Figure 7. As the number of spatial tokens decreases from 150 to 1, the occupancy reconstruction IoU exhibits only a marginal degradation, while inference efficiency improves significantly, with a 26% increase in FPS for a single spatial token. These results show a favorable trade-off between reconstruction quality and efficiency. Notably, the success rate on the point-goal navigation benchmark achieved with a single spatial token is comparable to, or slightly higher than, larger token sets. We conjecture that this compact single-token representation not only preserves the essential spatial information required for navigation, but also encourages the model to distill the most task-relevant spatial cues, thereby benefiting downstream decision-making.

VII. CONCLUSION

In this paper, we presented SPAN-Nav, an end-to-end embodied framework designed for generalized 3D spatial awareness. By compressing continuous scene representations into a single spatial token and employing a spatial-aware Chain-of-Thought (CoT), we enabled explicit and efficient integration of 3D spatial cues into action reasoning. Experimental results on our large-scale occupancy dataset demonstrated that SPAN-Nav significantly enhances navigation performance and gener-

alization across complex environments. Ultimately, this work addresses critical 3D perception bottlenecks and establishes a robust perceptual prior for tasks where expensive occupancy annotations are unavailable.

In future work, we aim to extend SPAN-Nav to cross-embodiment scenarios by bridging the perceptual gaps caused by varying robot kinematics and sensor layouts, further broadening the applicability of our spatial awareness framework.

VIII. APPENDIX

A. Encoder and Decoder Initialization

Following prior work on vector-quantized representation learning for occupancy reconstruction, we employ a Vector-Quantized Variational Autoencoder (VQ-VAE) to pretrain the occupancy encoder and decoder used in SPAN-Nav. Given a binary occupancy map $\mathbf{O}_t \in \{0, 1\}^{H \times W \times D}$, we treat it as a 2D feature map $\mathbf{x}_t \in \mathbb{R}^{D \times H \times W}$, where the height dimension is interpreted as the channel dimension.

A standard 2D ResNet-UNet style encoder extracts latent features \mathbf{z}_t , which are vector-quantized into discrete code indices and quantized representations \mathbf{z}_t^q via a learnable codebook. A 2D decoder then reconstructs occupancy logits $\tilde{\mathbf{y}}_t \in \mathbb{R}^{D \times H \times W}$.

The VQ-VAE is trained with a multi-term objective:

$$\mathcal{L} = \lambda_c \mathcal{L}_c + \lambda_l \mathcal{L}_l + \lambda_{vq} \mathcal{L}_{vq}, \quad (10)$$

where $\lambda_c, \lambda_l, \lambda_{vq}$ represent the hyperparameters for the occupancy reconstruction loss \mathcal{L}_c , Lovasz-hinge loss \mathcal{L}_l , and vector-quantization loss \mathcal{L}_{vq} , respectively, each of which is detailed in the subsequent discussion.

Let $o_i \in \mathbb{R}$ denote the predicted occupancy logit at voxel i and $y_i \in \{0, 1\}$ is the corresponding ground-truth label. The binary cross entropy loss for occupancy reconstruction is defined as

$$\mathcal{L}_c = -\frac{1}{N} \sum_{i=1}^N [y_i \log \sigma(o_i) + (1 - y_i) \log (1 - \sigma(o_i))], \quad (11)$$

where $\sigma(\cdot)$ denotes the sigmoid function and N is the total number of voxels.

To better optimize the intersection-over-union (IoU) metric, we follow previous works and apply the Lovasz-hinge loss:

$$\mathcal{L}_l = \bar{\Delta}_{\text{IoU}}(\text{sort}(1 - o_i y_i)), \quad (12)$$

where $\text{sort}(\cdot)$ denotes sorting in descending order and $\bar{\Delta}_{\text{IoU}}(\cdot)$ is the Lovasz extension of the IoU loss. The binary cross entropy loss and the Lovasz-hinge loss are also applied in the training of SPAN-Nav.

To regularize the latent space, the vector-quantization module employs a standard codebook and a commitment loss \mathcal{L}_{vq} . We first optimize the VQ-VAE on a large-scale annotated occupancy dataset; the resulting encoder and decoder are subsequently leveraged to facilitate the end-to-end training of the full SPAN-Nav framework.

B. Trajectory Generation for Point Goal Navigation

1) **Overview:** To generate collision-free navigation trajectories, we first discretize the i -th scene into a structured 3D representation. Specifically, we convert the scene into a set of H height-sliced occupancy maps $\mathbf{O}_i = \{\mathbf{o}_{i,k}\}_{k=1}^H$, where each slice $\mathbf{o}_{i,k}$ encodes binary occupancy within the height interval $[k\Delta z, (k+1)\Delta z)$. We use a cell size of 0.05 m and a height interval $\Delta z = 0.1$ m. To account for the robot's physical dimensions, we fuse all slices below the robot height threshold ($z_{\text{limit}} = 0.7$ m) into a 2D traversability map \mathbf{O}_{trav} , defined for each grid cell (x, y) as

$$\mathbf{O}_{\text{trav}}(x, y) = \bigvee_{k=0}^{\lfloor z_{\text{limit}}/\Delta z \rfloor - 1} \mathbf{o}_{i,k}(x, y), \quad (13)$$

where \bigvee denotes an element-wise logical OR over height slices. $\mathbf{O}_{\text{trav}}(x, y) = 1$ indicates the cell is occupied in at least one low-height slice and is thus non-traversable. Here (x, y) denotes the planar coordinates of a grid cell in the world frame (with resolution 0.05 m per cell). Based on \mathbf{O}_{trav} , we derive two planning primitives: (i) a roadmap graph $G = (V, E)$ constructed in free space and (ii) a distance-to-obstacle field D used as a clearance prior. In G , V is the set of roadmap nodes (2D positions sampled in traversable free space) and E is the set of collision-free edges connecting nearby nodes.

On top of these primitives, we generate trajectories with an online *A*+VO fusion* planner: *A** provides global guidance on the roadmap, while a Velocity-Obstacles (VO) controller performs local collision avoidance and outputs executable motions. The resulting trajectory is a sequence of robot poses

$$\tau = \{(x_t, y_t, \text{yaw}_t)\}_{t=0}^T, \quad (14)$$

where (x_t, y_t) denotes the robot's planar position in the world frame at time step t , and yaw_t is its heading angle (rotation about the vertical z -axis). In the following, we describe the design of the *A** component and the VO component, and how they are fused into an efficient online planner.

2) **Global Guidance via Roadmap *A**:** We run *A** on a roadmap built in the known map constructed on the current robot's observation. This produces a lightweight global guide that updates online as newly observed areas become available.

Known Map Construction. We maintain a three-state known map $\mathbf{M}_{\text{known}}$ (*free/occupied/unknown*) by accumulating the robot's observations over time (from $[-2\text{m}, 4\text{m}]$ in x -axis, and $[-2\text{m}, 2\text{m}]$ in y -axis). During *A** planning, unknown is treated as free to encourage optimistic exploration. Every K control steps, we filter the roadmap using the current $\mathbf{M}_{\text{known}}$ and re-run *A** to obtain an updated waypoint path $\tau^* = \{q_m\}_{m=0}^M$, where each waypoint $q_m = (x_m, y_m)$ is a 2D position in the world frame.

***A** Cost.** To bias the global guide away from walls and narrow passages, we incorporate the distance-to-obstacle field D into the *A** edge cost. For an edge $e = (i, j) \in E$ connecting roadmap nodes p_i and p_j , we define the cost

$$w(e) = \|p_i - p_j\| + \lambda \max(0, d_{\text{pref}} - d_{\text{min}}(e)), \quad (15)$$

where $\|p_i - p_j\|$ is the Euclidean edge length, $d_{\min}(e)$ is the minimum value of D on the straight-line segment from p_i to p_j , and d_{pref} is a user-defined preferred clearance threshold. This cost favors short edges while adding extra penalty to edges whose clearance is below d_{pref} , thereby encouraging A* to select routes that keep a larger safety margin from static obstacles.

A*-guided Local Goal Selection. Let $\tau^* = [q_0, \dots, q_M]$ denote the current A*-planned waypoint sequence, where each waypoint $q_m = (x_m, y_m)$ is a 2D position on the roadmap. Instead of tracking the next waypoint greedily, we select the **farthest** waypoint on τ^* that is reachable by a straight line-of-sight segment as the VO local goal g_{local} . This choice reduces oscillations and provides a stable directional target for local control.

3) **Local Avoidance via Truncated VO:** Given g_{local} from A*, the VO controller chooses a short-horizon control that is *provably safe* (hard constraints) and *preferentially high-clearance* (soft objective), producing smooth motions while reacting to dynamic obstacles in real time.

Robot modeling for VO. Since VO is formulated in velocity space, we approximate the robot footprint by an *oriented rectangle* of length L and width W (i.e., a rectangle whose orientation follows the robot heading yaw). Let $\{r^c\}_{c=1}^4$ be the four rectangle corners expressed in the robot frame. For a candidate holonomic control $u = (v_x, v_y, \omega)$, where (v_x, v_y) is the translational velocity in the robot frame and ω is the yaw-rate command, the induced world-frame velocity of corner c is approximated as

$$v^c = R(\text{yaw}) [v_x, v_y]^\top + \omega \times r^c, \quad (16)$$

where $R(\text{yaw})$ rotates robot-frame velocities into the world frame and $\omega \times r^c$ is the tangential velocity at the corner due to rotation about the vertical axis. A candidate control is accepted only if all corner velocities satisfy the (truncated) VO constraints for dynamic obstacles, and the corresponding short-horizon rollout does not collide with the static occupancy map.

Hard safety: truncated VO + lookahead checking. For each footprint corner c and each dynamic obstacle, we construct a truncated velocity-obstacle (VO) constraint with a finite horizon T_{VO} . In this way we reject only candidate motions that may lead to collision within T_{VO} (instead of the infinite-horizon VO). Let p^c be the corner position, and let the obstacle have center p^o and velocity v^o . We define the relative position and velocity as $p_{\text{rel}}^c = p^c - p^o$ and $v_{\text{rel}}^c = v^c - v^o$. A candidate is rejected if it is closing (with this definition, closing corresponds to $(p_{\text{rel}}^c)^\top v_{\text{rel}}^c > 0$), the relative-velocity direction lies inside the VO cone, and the relative speed is sufficient to reach the inflated obstacle within T_{VO} . In addition to the truncated VO, we perform a short-horizon forward rollout over T_{look} and reject candidates whose predicted motion collides with the static occupancy map or with predicted dynamic obstacle positions.

Soft preferences: tracking + smoothness + clearance. Among the safe candidates, we select the control $u =$

(v_x, v_y, ω) minimizing the weighted objective:

$$\begin{aligned} J(u) = & w_v \|v - v_{\text{des}}\| + w_{\text{curr}} \|v - v_{\text{curr}}\| - w_{\text{speed}} \|v\| \\ & + w_\omega |\omega - \omega_{\text{des}}| + J_{\text{stat}}(d_{\text{min}}^{\text{stat}}) + J_{\text{dyn}}(d_{\text{min}}^{\text{dyn}}) \\ & + w_a \|v\| (1 - \hat{v}^\top \hat{g}). \end{aligned} \quad (17)$$

where all w 's are non-negative scalar weights. Here $v = [v_x, v_y]^\top$ is the translational command (robot frame), v_{curr} is the current translational velocity, and $(v_{\text{des}}, \omega_{\text{des}})$ is the desired command derived from the local goal. The first two terms promote tracking and smoothness, while $-w_{\text{speed}} \|v\|$ mildly encourages forward progress. The terms $w_\omega |\omega - \omega_{\text{des}}|$ and $w_a \|v\| (1 - \hat{v}^\top \hat{g})$ favor smooth turning and goal-aligned motion, respectively. Here \hat{v} is the normalized velocity direction, and \hat{g} is the normalized direction from the robot to the local goal g_{local} (both in the world frame). We set v_{des} to be heading-aligned by default; if the heading error to g_{local} is large, we set $v_{\text{des}} = 0$ to enable in-place turning and compute ω_{des} from the heading error.

Let $d_{\text{min}}^{\text{stat}}$ be the minimum static clearance (queried from D along the rollout) after subtracting a footprint margin r_{eff} . We penalize low clearance only when it falls below a preferred threshold d_{pref} :

$$J_{\text{stat}} = \begin{cases} \frac{w_c}{d_{\text{min}}^{\text{stat}} + \epsilon_c}, & d_{\text{min}}^{\text{stat}} < d_{\text{pref}}, \\ 0, & \text{otherwise,} \end{cases} \quad (18)$$

where w_c is the clearance-penalty weight and ϵ_c is a small constant. Similarly, let $d_{\text{min}}^{\text{dyn}}$ be the minimum predicted clearance to dynamic obstacles over the lookahead horizon (subtracting obstacle radius plus r_{eff}). We penalize dynamic proximity more strongly:

$$J_{\text{dyn}} = \begin{cases} \frac{2w_c}{d_{\text{min}}^{\text{dyn}} + \epsilon_c}, & d_{\text{min}}^{\text{dyn}} < 1.5 d_{\text{pref}}, \\ 0, & \text{otherwise.} \end{cases} \quad (19)$$

Together, these terms make the controller naturally maintain a buffer from both static structures and moving agents, beyond merely avoiding collision.

4) **Summary:** Overall, the proposed A*+VO fusion planner enables efficient and reliable trajectory generation. By combining A*-based global guidance with truncated-VO local avoidance and distance-map clearance priors, it produces smooth, collision-free trajectories that naturally keep a safety buffer from obstacles. Moreover, the trajectories are strongly aligned with the spatial reasoning process: A* guidance is planned on a $\mathbf{M}_{\text{known}}$ that is incrementally built from the same receptive field used to construct occupancy labels. Consequently, the explored/free/occupied structure that drives A* planning matches the occ labeling frame, yielding trajectories that are naturally consistent with our spatial Chain-of-Thought supervision.

C. Trajectory Generation for FrodoBots-2K Data

The FrodoBots-2K dataset was collected using low-cost onboard sensors, including wheel encoders and a magnetometer, resulting in limited observability and pronounced drift in

the raw trajectories. To obtain reliable action supervision, we perform 2D trajectory reconstruction using a dead-reckoning pipeline that exploits motion constraints and absolute heading observations. Linear velocity is estimated from wheel encoder measurements, while zero-velocity updates (ZUPT) are applied during detected stationary intervals to enforce kinematic consistency and regularize motion estimation. These zero-motion constraints improve the system’s observability and are further used to suppress magnetometer-induced heading drift during low-dynamics periods. Magnetometer measurements, after hard-iron calibration, provide absolute heading observations and are fused using a Kalman filter with a state vector $[yaw, yaw_rate]$ under a constant angular velocity model. To reduce accumulated drift and improve temporal consistency, Rauch–Tung–Striebel (RTS) smoothing is applied over the heading estimates. Finally, the smoothed heading and regularized linear velocity are integrated to produce refined 2D trajectories, which serve as stable supervision for real-world navigation learning.

D. Occupancy Annotation for Real World

We generate occupancy ground truth using a feed-forward depth reconstruction pipeline based on Depth Anything V3. Depth is jointly predicted from the current RGB frame and a temporally adjacent frame (1 s later) to improve geometric stability under sparse viewpoints. The predicted depth is converted into a 3D point cloud, from which ground and non-ground regions are separated via normal-based filtering and RANSAC plane fitting. Points whose surface normals are within 30° of the vertical axis are treated as ground candidates. The segmented point cloud is then voxelized using the same resolution, spatial extent, and coordinate conventions as the PointGoal Navigation benchmark. Occupancy labels are finally obtained through ray casting based on the camera pose and field of view.

E. QA Loss and Two-Stage Training Strategy

In the QA setting, the model leverages a vision-language architecture to predict answers derived from the provided image and query. We employ a standard cross-entropy loss to supervise the model, measuring the divergence between the predicted and actual labels as follows:

$$\mathcal{L}_{qa} = - \sum_{i=1}^N \mathbf{y}_i \log(\mathbf{P}(\hat{\mathbf{y}}_i)),$$

where \mathbf{y}_i denotes the ground-truth answer in a one-hot encoded format, and $\hat{\mathbf{y}}_i$ represents the predicted probability distribution typically computed via a softmax activation function. Here, $\mathbf{P}(\hat{\mathbf{y}}_i)$ signifies the probability assigned by the model to each constituent token, with N indicating the total number of words in the generated response.

In the two-stage training process, QA loss plays a critical role in improving the language understanding capacity of the model, as well as its ability to reason about the physical world. In the first stage, we train the model using 2 million trajectories

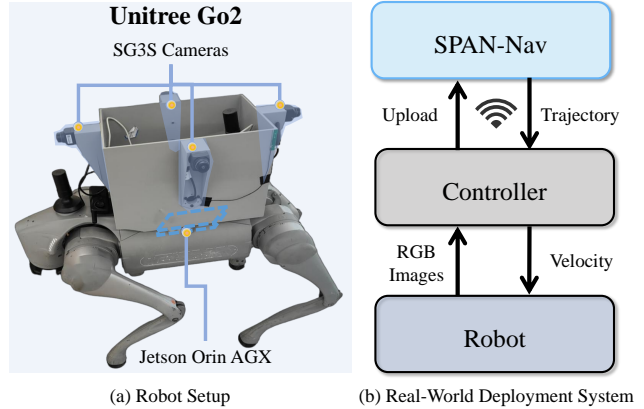


Fig. 8: **Physical platform architecture.** (a) Computation unit (Jetson Orin AGX), and sensors. (b) Information flow and data pipeline during real-world deployment.

annotated with occupancy information and 0.5 million QA samples. In the second stage, we further train the model on the full set of trajectory and QA data. Through this two-stage training strategy, the model acquires generalized spatial perception capabilities, which subsequently enable accurate trajectory prediction.

In particular, to evaluate the model’s ability to generalize across different agents, as discussed in SPAN-Nav Generalize, we do not use occupancy annotations from the VLN data set at any stage of training.

F. Real World Setting

To validate the generalization capability of SPAN-Nav, we perform various task-based evaluations in real-world environments; for comprehensive experimental details, please refer to the supplementary video. In real-world deployments, our model acts as a general Visual-Language-Action (VLA) controller capable of driving real embodiments. As illustrated in Figure 8, the system takes visual observations—obtained from one or more cameras—along with language instructions to directly predict a trajectory. We then leverage embodiment-specific APIs to navigate the robot along the predicted path. Notably, the integration of Lidar is optional in our framework. While the supplementary video showcases instances of fully autonomous navigation relying solely on visual perception, we proactively enable Lidar as a supplementary safety layer in highly congested areas with dense pedestrian traffic to prioritize the safety of bystanders. Specifically, our model is hosted on a remote server featuring an NVIDIA GeForce RTX 4090 GPU, communicating with robotic clients via the Internet. The robots transmit compressed observations to the server, which then processes them to output trajectories that the local planners subsequently translate into low-level commands, such as velocity or joint controls.

G. Simulator Result

To further demonstrate the effectiveness of our approach, we provide additional experimental visualizations in unseen environments. As illustrated in Figure 11, we present several

PointGoal Navigation

Instruction: Go to the position of $x:[0.4], y:[-1.65]$.

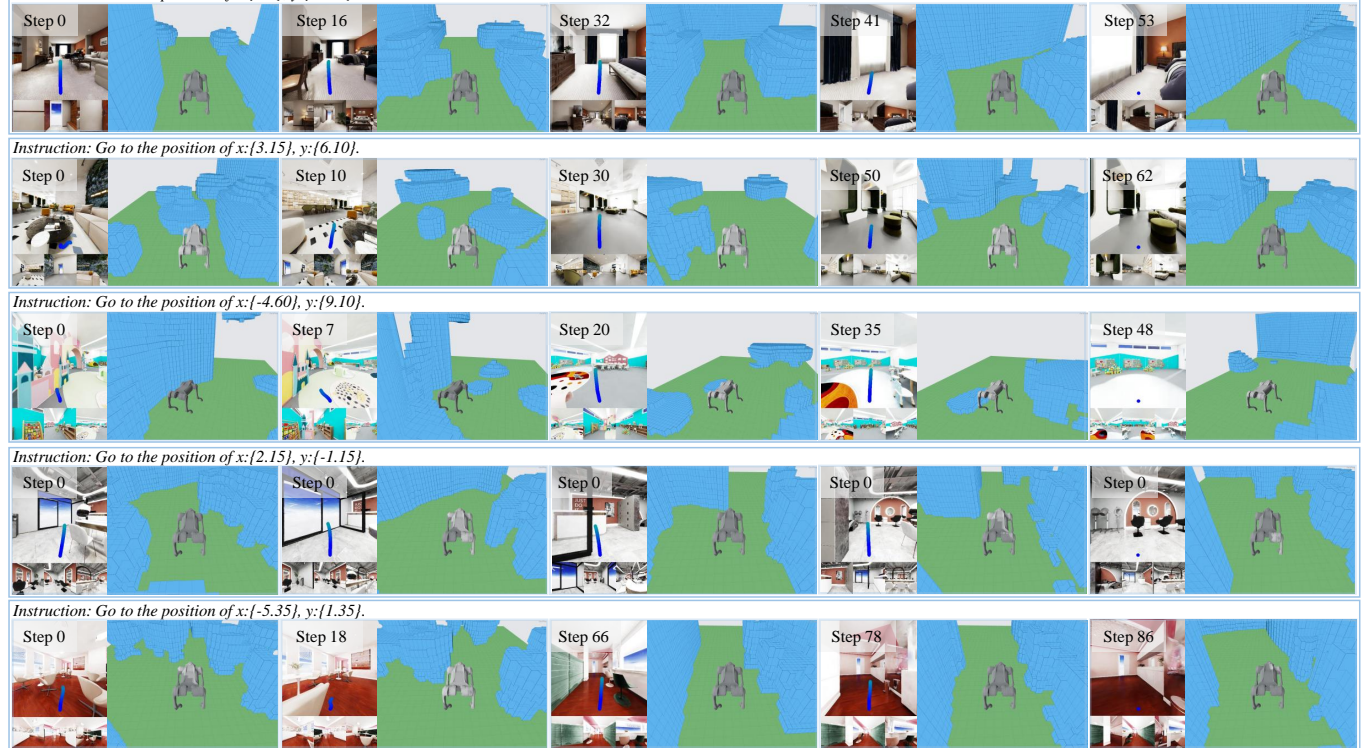


Fig. 9: Experimental Visualization of SPAN-Nav for PointGoal Navigation.

Urban Navigation

Instruction: Move to the next series of target points according to the city walking navigation (0, 2), ..., (86, 40).

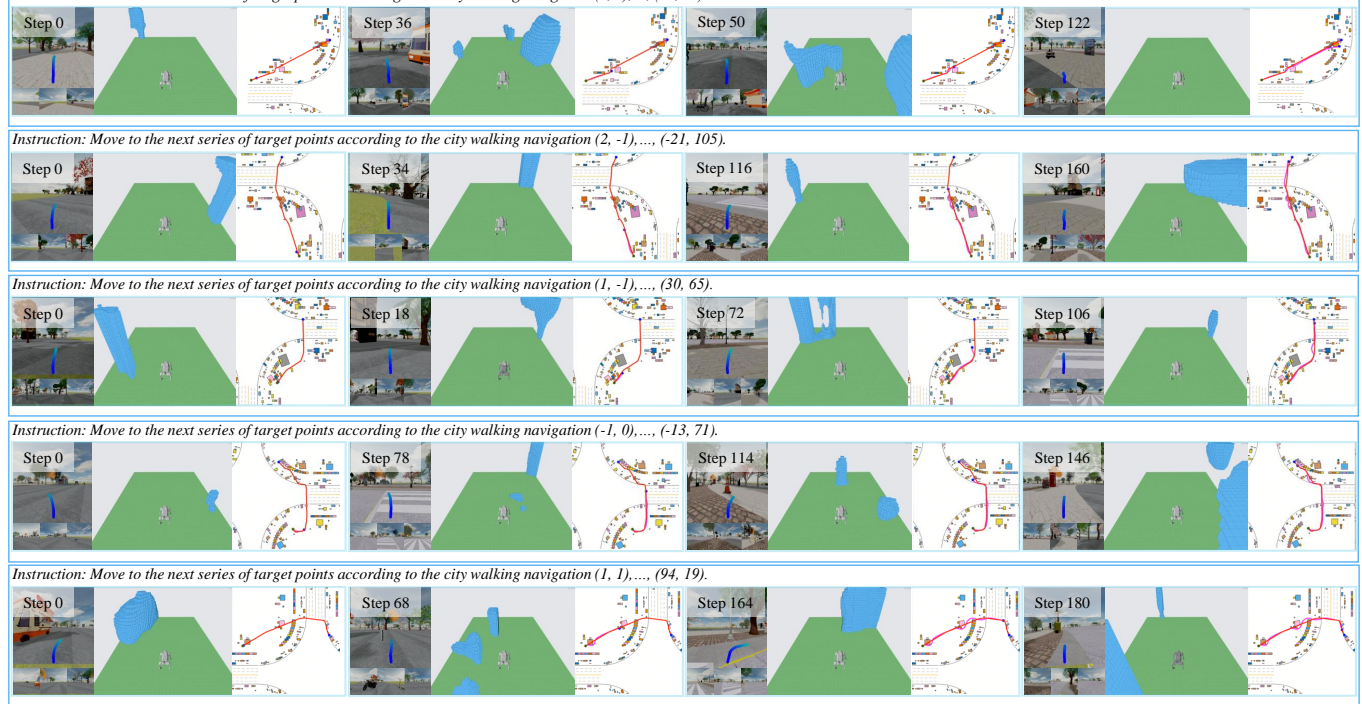
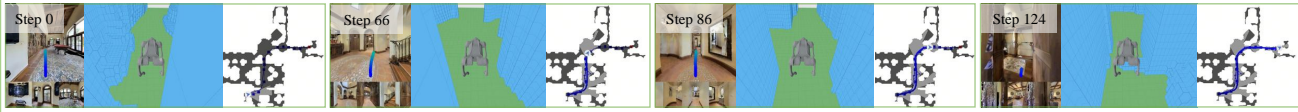


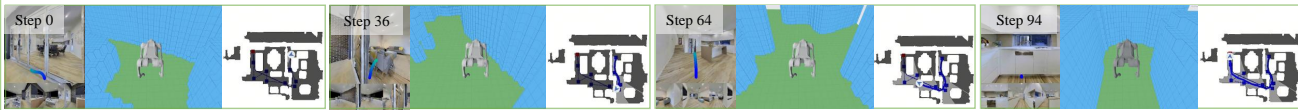
Fig. 10: Experimental Visualization of SPAN-Nav for Urban Navigation.

Vision-and-Language Navigation

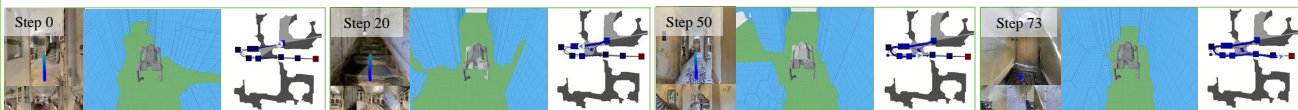
Instruction: You will start by facing the pool table. On the left side of the pool table there is a large opening. Walk towards the opening. Once you are inside you will see the living room on your left and lounge area on your right. Just ahead of you there's an arched opening. Walk towards that. Once you are here you will see a round tiled floors. Take a step to the right you will see the staircase on your right and just next to the staircase there is an opening. Walk inside the opening. You will see another round area. Exactly in front of you there is an arched opening that lead to a bedroom. Walk towards the opening and inside the bedroom. Continue to walk forward passing the bed and towards a narrow opening. Here you will see an empty closet and you're done.



Instruction: You're now facing the glass door. Turn left and walk straight towards the white colour table on your left side. From there, turn right and enter the glass door. Move forward towards the refrigerator and turn right. Now walk straight till you reach the white colour cabinet. Stop near the washbasin, you will reach your destination.



Instruction: Turn left towards the open door and exit the room and walk straight towards the steps and walk up the steps, turn left and walk up the steps and walk straight along the narrow path and move straight towards the end of the closed door and you have reached your destination.



Instruction: You're now facing the wooden cabinet. Turn around and walk towards the plant and then take right. Now walk straight, exit the glass door and take left. You will see the stairs in front of you. Walk in front of the stairs till you reach the white colour mat and then take right. Now walk straight where a glass table with multiple white colour chairs are placed. Walk in between the white colour chairs and the white cabinet on your right side. Walk straight and get in to the room where you will see a washbasin. Turn right just before the washbasin and walk straight completely till you see a white colour sofa on your left side. Go near the white colour sofa and stand in front of the lamp where you can also see a coffee cup. Stand in front of the lamp, you will reach your destination.



Instruction: Move forward from the place you are standing and exit the room, turn left and move forward, you can find steps to your left, go up the steps, you can find two steps in front of you, go up the steps, stand at the entrance of the second room which is to your right, that would be your end point.



Fig. 11: Experimental Visualization of SPAN-Nav for VLN.

examples from Vision-and-Language Navigation (VLN) tasks. Under long-horizon instructions, the agent predicts plausible occupancy maps that encompass traversable doors and intersections. Leveraging such explicit spatial reasoning, the agent executes navigation tasks seamlessly.

Similarly, Figure 9 evaluates the performance of SPAN-Nav in PointGoal Navigation. The agent infers the 3D occupancy of surrounding obstacles and plans collision-free trajectories to reach the goal location. Furthermore, Figure 10 showcases the verification results in outdoor Urban Navigation, where SPAN-Nav efficiently predicts structural elements such as buildings, vegetation, and vehicles, leading to a substantial improvement in the task completion.

Notably, by introducing the spatial Chain-of-Thought mechanism, the compact spatial token learns a more navigation-critical occupancy representation, rather than optimizing purely for pixel-wise reconstruction accuracy. Specifically, complex articulated structures such as swivel chairs and shelves are reconstructed as holistic, non-traversable obstacles, instead of being decomposed into fine-grained geometric details. While this abstraction facilitates easier reasoning over spatial structure for navigation and action planning, it sacrifices some geometric fidelity, leading to a slight decrease in occupancy reconstruction IoU, as observed in the ablation study.

REFERENCES

- [1] Jiazhao Zhang, Anqi Li, Yunpeng Qi, Minghan Li, Jiahang Liu, Shaoan Wang, Haoran Liu, Gengze Zhou, Yuze Wu, Xingxing Li, et al. Embodied navigation foundation model. *arXiv preprint arXiv:2509.12129*, 2025.
- [2] Jiazhao Zhang, Kunyu Wang, Shaoan Wang, Minghan Li, Haoran Liu, Songlin Wei, Zhongyuan Wang, Zhizheng Zhang, and He Wang. Uni-navid: A video-based vision-language-action model for unifying embodied navigation tasks. *arXiv preprint arXiv:2412.06224*, 2024.
- [3] Jiazhao Zhang, Kunyu Wang, Rongtao Xu, Gengze Zhou, Yicong Hong, Xiaomeng Fang, Qi Wu, Zhizheng Zhang, and He Wang. Navid: Video-based vlm plans the next step for vision-and-language navigation. *Robotics: Science and Systems*, 2024.
- [4] Shaoan Wang, Jiazhao Zhang, Minghan Li, Jiahang Liu, Anqi Li, Kui Wu, Fangwei Zhong, Junzhi Yu, Zhizheng Zhang, and He Wang. Trackvla: Embodied visual tracking in the wild. *arXiv preprint arXiv:2505.23189*, 2025.
- [5] Tianyu Xu, Jiawei Chen, Jiazhao Zhang, Wenyao Zhang, Zekun Qi, Minghan Li, Zhizheng Zhang, and He Wang. Mm-nav: Multi-view vla model for robust visual navigation via multi-expert learning. *arXiv preprint arXiv:2510.03142*, 2025.
- [6] Intern Robotics. Internvla-n1: An open dual-system

- vision-language navigation foundation model with learned latent plans. 2025.
- [7] Tairan He, Chong Zhang, Wenli Xiao, Guanqi He, Changliu Liu, and Guanya Shi. Agile but safe: Learning collision-free high-speed legged locomotion. *arXiv preprint arXiv:2401.17583*, 2024.
- [8] Matthew Chang, Theophile Gervet, Mukul Khanna, Sriram Yenamandra, Dhruv Shah, So Yeon Min, Kavitha Shah, Chris Paxton, Saurabh Gupta, Dhruv Batra, et al. Goat: Go to any thing. *arXiv preprint arXiv:2311.06430*, 2023.
- [9] Abdelrhman Werby, Chenguang Huang, Martin Büchner, Abhinav Valada, and Wolfram Burgard. Hierarchical open-vocabulary 3d scene graphs for language-grounded robot navigation. In *First Workshop on Vision-Language Models for Navigation and Manipulation at ICRA 2024*, 2024.
- [10] Wenzhe Cai, Jiaqi Peng, Yuqiang Yang, Yujian Zhang, Meng Wei, Hanqing Wang, Yilun Chen, Tai Wang, and Jiangmiao Pang. Navdp: Learning sim-to-real navigation diffusion policy with privileged information guidance. *arXiv preprint arXiv:2505.08712*, 2025.
- [11] Zifan Wang, Teli Ma, Yufei Jia, Xun Yang, Jiaming Zhou, Wenlong Ouyang, Qiang Zhang, and Junwei Liang. Omni-perception: Omnidirectional collision avoidance for legged locomotion in dynamic environments. *arXiv preprint arXiv:2505.19214*, 2025.
- [12] Wenzhao Zheng, Weiliang Chen, Yuanhui Huang, Borui Zhang, Yueqi Duan, and Jiwen Lu. Occworld: Learning a 3d occupancy world model for autonomous driving. In *European conference on computer vision*, pages 55–72. Springer, 2024.
- [13] Lening Wang, Wenzhao Zheng, Yilong Ren, Han Jiang, Zhiyong Cui, Haiyang Yu, and Jiwen Lu. Occsora: 4d occupancy generation models as world simulators for autonomous driving. *arXiv preprint arXiv:2405.20337*, 2024.
- [14] Julong Wei, Shanshuai Yuan, Pengfei Li, Qingda Hu, Zhongxue Gan, and Wenchao Ding. Occllama: An occupancy-language-action generative world model for autonomous driving. *arXiv preprint arXiv:2409.03272*, 2024.
- [15] Yuanhui Huang, Wenzhao Zheng, Yunpeng Zhang, Jie Zhou, and Jiwen Lu. Tri-perspective view for vision-based 3d semantic occupancy prediction. In *Proceedings of the IEEE/CVF conference on computer vision and pattern recognition*, pages 9223–9232, 2023.
- [16] Zhang Zhang, Qiang Zhang, Wei Cui, Shuai Shi, Yijie Guo, Gang Han, Wen Zhao, Jingkai Sun, Jiahang Cao, Jiayu Wang, et al. Occupancy world model for robots. *arXiv preprint arXiv:2505.05512*, 2025.
- [17] Yili Liu, Linzhan Mou, Xuan Yu, Chenrui Han, Sitong Mao, Rong Xiong, and Yue Wang. Let occ flow: Self-supervised 3d occupancy flow prediction. *arXiv preprint arXiv:2407.07587*, 2024.
- [18] Ruixun Liu, Lingyu Kong, Derun Li, and Hang Zhao. Occvla: Vision-language-action model with implicit 3d occupancy supervision. *arXiv preprint arXiv:2509.05578*, 2025.
- [19] Tianshuo Xu, Hao Lu, Xu Yan, Yingjie Cai, Bingbing Liu, and Yingcong Chen. Occ-llm: Enhancing autonomous driving with occupancy-based large language models. *arXiv preprint arXiv:2502.06419*, 2025.
- [20] Aaron Van Den Oord, Oriol Vinyals, et al. Neural discrete representation learning. *Advances in neural information processing systems*, 30, 2017.
- [21] Santhosh K Ramakrishnan, Aaron Gokaslan, Erik Wijmans, Oleksandr Maksymets, Alex Clegg, John Turner, Eric Undersander, Wojciech Galuba, Andrew Westbury, Angel X Chang, et al. Habitat-matterport 3d dataset (hm3d): 1000 large-scale 3d environments for embodied ai. *arXiv preprint arXiv:2109.08238*, 2021.
- [22] Wayne Wu, Honglin He, Jack He, Yiran Wang, Chenda Duan, Zhizheng Liu, Quanyi Li, and Bolei Zhou. Metaurban: An embodied ai simulation platform for urban micromobility. In *The Thirteenth International Conference on Learning Representations*, 2025.
- [23] Bingchen Miao, Rong Wei, Zhiqi Ge, Shiqi Gao, Jingzhe Zhu, Renhan Wang, Siliang Tang, Jun Xiao, Rui Tang, Juncheng Li, et al. Towards physically executable 3d gaussian for embodied navigation. *arXiv preprint arXiv:2510.21307*, 2025.
- [24] Anqi Li, Zhiyong Wang, Jiazhao Zhang, Minghan Li, Yunpeng Qi, Zhibo Chen, Zhizheng Zhang, and He Wang. Urbanvla: A vision-language-action model for urban micromobility. *arXiv preprint arXiv:2510.23576*, 2025.
- [25] Alexander Ku, Peter Anderson, Roma Patel, Eugene Ie, and Jason Baldridge. Room-across-room: Multilingual vision-and-language navigation with dense spatiotemporal grounding. In *Proceedings of the 2020 Conference on Empirical Methods in Natural Language Processing (EMNLP)*, pages 4392–4412, 2020.
- [26] Weipeng Zhong, Peizhou Cao, Yichen Jin, Li Luo, Wenzhe Cai, Jingli Lin, Hanqing Wang, Zhaoyang Lyu, Tai Wang, Bo Dai, et al. Internscenes: A large-scale simulatable indoor scene dataset with realistic layouts. *arXiv preprint arXiv:2509.10813*, 2025.
- [27] Manolis Savva, Abhishek Kadian, Oleksandr Maksymets, Yili Zhao, Erik Wijmans, Bhavana Jain, Julian Straub, Jia Liu, Vladlen Koltun, Jitendra Malik, Devi Parikh, and Dhruv Batra. Habitat: A Platform for Embodied AI Research. *ICCV*, 2019.
- [28] NVIDIA. Isaac Sim. URL <https://github.com/isaac-sim/IsaacSim>.
- [29] Jacob Krantz, Erik Wijmans, Arjun Majumdar, Dhruv Batra, and Stefan Lee. Beyond the nav-graph: Vision-and-language navigation in continuous environments. In *European Conference on Computer Vision*, pages 104–120. Springer, 2020.
- [30] Jungdae Lee, Taiki Miyanishi, Shuhei Kurita, Koya Sakamoto, Daichi Azuma, Yutaka Matsuo, and Nakamasa Inoue. Citynav: Language-goal aerial navigation

- dataset with geographic information, 2024.
- [31] Xiangyu Wang, Donglin Yang, Ziqin Wang, Hohin Kwan, Jinyu Chen, Wenjun Wu, Hongsheng Li, Yue Liao, and Si Liu. Towards realistic uav vision-language navigation: Platform, benchmark, and methodology. *arXiv preprint arXiv:2410.07087*, 2024.
- [32] Gengze Zhou, Yicong Hong, and Qi Wu. Navgpt: Explicit reasoning in vision-and-language navigation with large language models. *arXiv preprint arXiv:2305.16986*, 2023.
- [33] Dhruv Shah, Blazej Osinski, Brian Ichter, and Sergey Levine. Lm-nav: Robotic navigation with large pre-trained models of language, vision, and action. *arXiv preprint arXiv:2207.04429*, 2022.
- [34] Yanyuan Qiao, Yuankai Qi, Zheng Yu, Jing Liu, and Qi Wu. March in chat: Interactive prompting for remote embodied referring expression. In *Proceedings of the IEEE/CVF International Conference on Computer Vision*, pages 15758–15767, 2023.
- [35] Bowen Pan, Rameswar Panda, SouYoung Jin, Rogerio Feris, Aude Oliva, Phillip Isola, and Yoon Kim. Langnav: Language as a perceptual representation for navigation. *arXiv preprint arXiv:2310.07889*, 2023.
- [36] Yuxing Long, Xiaoqi Li, Wenzhe Cai, and Hao Dong. Discuss before moving: Visual language navigation via multi-expert discussions. *arXiv preprint arXiv:2309.11382*, 2023.
- [37] Bingqian Lin, Yunshuang Nie, Ziming Wei, Jiaqi Chen, Shikui Ma, Jianhua Han, Hang Xu, Xiaojun Chang, and Xiaodan Liang. Navcot: Boosting llm-based vision-and-language navigation via learning disentangled reasoning. *IEEE Transactions on Pattern Analysis and Machine Intelligence*, 2025.
- [38] Jiaqi Chen, Bingqian Lin, Ran Xu, Zhenhua Chai, Xiaodan Liang, and Kwan-Yee K Wong. Mapgpt: Map-guided prompting for unified vision-and-language navigation. *arXiv preprint arXiv:2401.07314*, 2024.
- [39] Yanyuan Qiao, Wenqi Lyu, Hui Wang, Zixu Wang, Zerui Li, Yuan Zhang, Mingkui Tan, and Qi Wu. Opennav: Exploring zero-shot vision-and-language navigation in continuous environment with open-source llms. In *2025 IEEE International Conference on Robotics and Automation (ICRA)*, pages 6710–6717. IEEE, 2025.
- [40] An-Chieh Cheng, Yandong Ji, Zhaojing Yang, Xueyan Zou, Jan Kautz, Erdem Biyik, Hongxu Yin, Sifei Liu, and Xiaolong Wang. Navila: Legged robot vision-language-action model for navigation. In *RSS*, 2025.
- [41] Meng Wei, Chenyang Wan, Xiqian Yu, Tai Wang, Yuqiang Yang, Xiaohan Mao, Chenming Zhu, Wenzhe Cai, Hanqing Wang, Yilun Chen, et al. Streamvln: Streaming vision-and-language navigation via slowfast context modeling. *arXiv preprint arXiv:2507.05240*, 2025.
- [42] Gengze Zhou, Yicong Hong, Zun Wang, Xin Eric Wang, and Qi Wu. Navgpt-2: Unleashing navigational reasoning capability for large vision-language models. In *Euro-pean Conference on Computer Vision*, pages 260–278. Springer, 2025.
- [43] Duo Zheng, Shijia Huang, Lin Zhao, Yiwu Zhong, and Liwei Wang. Towards learning a generalist model for embodied navigation. In *Proceedings of the IEEE/CVF Conference on Computer Vision and Pattern Recognition*, pages 13624–13634, 2024.
- [44] Lingfeng Zhang, Xiaoshuai Hao, Qinwen Xu, Qiang Zhang, Xinyao Zhang, Pengwei Wang, Jing Zhang, Zhongyuan Wang, Shanghang Zhang, and Renjing Xu. MapNav: A novel memory representation via annotated semantic maps for VLM-based vision-and-language navigation. In *Proceedings of the 63rd Annual Meeting of the Association for Computational Linguistics*, pages 13032–13056, July 2025.
- [45] Gengze Zhou, Yicong Hong, Zun Wang, Chongyang Zhao, Mohit Bansal, and Qi Wu. Same: Learning generic language-guided visual navigation with state-adaptive mixture of experts. *arXiv preprint arXiv:2412.05552*, 2024.
- [46] Hanqing Wang, Wei Liang, Luc V Gool, and Wenguan Wang. Towards versatile embodied navigation. *Advances in neural information processing systems*, 35:36858–36874, 2022.
- [47] Yuxing Long, Wenzhe Cai, Hongcheng Wang, Guanqi Zhan, and Hao Dong. Instructnav: Zero-shot system for generic instruction navigation in unexplored environment. *arXiv preprint arXiv:2406.04882*, 2024.
- [48] Xinshuai Song, Weixing Chen, Yang Liu, Weikai Chen, Guanbin Li, and Liang Lin. Towards long-horizon vision-language navigation: Platform, benchmark and method. In *Proceedings of the Computer Vision and Pattern Recognition Conference*, pages 12078–12088, 2025.
- [49] Chen Gao, Liankai Jin, Xingyu Peng, Jiazhao Zhang, Yue Deng, Annan Li, He Wang, and Si Liu. Octonav: Towards generalist embodied navigation. *arXiv preprint arXiv:2506.09839*, 2025.
- [50] Hang Yin, Xiuwei Xu, Linqing Zhao, Ziwei Wang, Jie Zhou, and Jiwen Lu. Unigoal: Towards universal zero-shot goal-oriented navigation. In *Proceedings of the Computer Vision and Pattern Recognition Conference*, pages 19057–19066, 2025.
- [51] Shouwei Ruan, Liyuan Wang, Caixin Kang, Qihui Zhu, Songming Liu, Xingxing Wei, and Hang Su. From reactive to cognitive: brain-inspired spatial intelligence for embodied agents. *arXiv preprint arXiv:2508.17198*, 2025.
- [52] An-Qi Cao and Renaud De Charette. Monoscene: Monocular 3d semantic scene completion. In *Proceedings of the IEEE/CVF Conference on Computer Vision and Pattern Recognition*, pages 3991–4001. IEEE/CVF, 2022.
- [53] Yang Wei, Lin Zhao, Wenzhao Zheng, Zeyu Zhu, Jiaya Zhou, and Jiwen Lu. Surroundocc: Multi-camera 3d occupancy prediction for autonomous driving. In *Proceedings of the IEEE/CVF International Conference on*

- Computer Vision*, pages 21729–21740. IEEE/CVF, 2023.
- [54] Xiaotian Tian, Tiancheng Jiang, Lin Yun, Yihong Mao, Hao Yang, Yuchen Wang, Yixuan Wang, and Hang Zhao. Occ3d: A large-scale 3d occupancy prediction benchmark for autonomous driving. *Advances in Neural Information Processing Systems*, 36:64318–64330, 2023.
- [55] Xiaosong Wang, Zeyu Zhu, Wenbo Xu, Yifan Zhang, Yang Wei, Xiaojuan Chi, Yan Ye, Dalong Du, Jiwen Lu, and Xinggang Wang. Openoccupancy: A large scale benchmark for surrounding semantic occupancy perception. In *Proceedings of the IEEE/CVF International Conference on Computer Vision*, pages 17850–17859. IEEE/CVF, 2023.
- [56] Zetong Li, Zhiding Yu, Drew Austin, Meng Fang, Shiyi Lan, Jan Kautz, and Jose M. Alvarez. Fb-occ: 3d occupancy prediction based on forward-backward view transformation, 2023.
- [57] Yifan Zhang, Zeyu Zhu, and Dalong Du. Occformer: Dual-path transformer for vision-based 3d semantic occupancy prediction. In *Proceedings of the IEEE/CVF International Conference on Computer Vision*, pages 9433–9443. IEEE/CVF, 2023.
- [58] Ting Huang, Dongjian Li, Rui Yang, Zeyu Zhang, Zida Yang, and Hao Tang. Mobilevla-r1: Reinforcing vision-language-action for mobile robots. *arXiv preprint arXiv:2511.17889*, 2025.
- [59] Zhangyang Qi, Zhixiong Zhang, Yizhou Yu, Jiaqi Wang, and Hengshuang Zhao. Vln-r1: Vision-language navigation via reinforcement fine-tuning. *arXiv preprint arXiv:2506.17221*, 2025.
- [60] Qingqing Zhao, Yao Lu, Moo Jin Kim, Zipeng Fu, Zhuoyang Zhang, Yecheng Wu, Zhaoshuo Li, Qianli Ma, Song Han, Chelsea Finn, et al. Cot-vla: Visual chain-of-thought reasoning for vision-language-action models. In *Proceedings of the Computer Vision and Pattern Recognition Conference*, pages 1702–1713, 2025.
- [61] Shuai Bai, Yuxuan Cai, Ruizhe Chen, Keqin Chen, Xionghui Chen, Zesen Cheng, Lianghao Deng, Wei Ding, Chang Gao, Chunjiang Ge, Wenbin Ge, Zhifang Guo, Qidong Huang, Jie Huang, Fei Huang, Binyuan Hui, Shutong Jiang, Zhaohai Li, Mingsheng Li, Mei Li, Kaixin Li, Zicheng Lin, Junyang Lin, Xuejing Liu, Jiawei Liu, Chenglong Liu, Yang Liu, Dayiheng Liu, Shixuan Liu, Dunjie Lu, Ruilin Luo, Chenxu Lv, Rui Men, Lingchen Meng, Xuancheng Ren, Xingzhang Ren, Sibao Song, Yuchong Sun, Jun Tang, Jianhong Tu, Jianqiang Wan, Peng Wang, Pengfei Wang, Qiuyue Wang, Yuxuan Wang, Tianbao Xie, Yiheng Xu, Haiyang Xu, Jin Xu, Zhibo Yang, Mingkun Yang, Jianxin Yang, An Yang, Bowen Yu, Fei Zhang, Hang Zhang, Xi Zhang, Bo Zheng, Humen Zhong, Jingren Zhou, Fan Zhou, Jing Zhou, Yuanzhi Zhu, and Ke Zhu. Qwen3-vl technical report. *arXiv preprint arXiv:2511.21631*, 2025.
- [62] Jacob Devlin, Ming-Wei Chang, Kenton Lee, and Kristina Toutanova. Bert: Pre-training of deep bidirectional transformers for language understanding. In *Proceedings of the 2019 conference of the North American chapter of the association for computational linguistics: human language technologies, volume 1 (long and short papers)*, pages 4171–4186, 2019.
- [63] Stéphane Ross, Geoffrey Gordon, and Drew Bagnell. A reduction of imitation learning and structured prediction to no-regret online learning. In *Proceedings of the fourteenth international conference on artificial intelligence and statistics*, pages 627–635. JMLR Workshop and Conference Proceedings, 2011.
- [64] Zhen Li, Chuanhao Li, Xiaofeng Mao, Shaoheng Lin, Ming Li, Shitian Zhao, Zhaopan Xu, Xinyue Li, Yukang Feng, Jianwen Sun, et al. Sekai: A video dataset towards world exploration. *arXiv preprint arXiv:2506.15675*, 2025.
- [65] FrodoBots Lab. Frodobots-2k dataset. Hugging Face Datasets, sep 2025. URL <https://huggingface.co/datasets/frodoBots/FrodoBots-2K>. Updated: 2025-09-23; Accessed: 2025-08-04.
- [66] Bingchen Miao, Rong Wei, Zhiqi Ge, Xiaoquan sun, Shiqi Gao, Jingzhe Zhu, Renhan Wang, Siliang Tang, Jun Xiao, Rui Tang, and Juncheng Li. Towards physically executable 3d gaussian for embodied navigation, 2025. URL <https://arxiv.org/abs/2510.21307>.
- [67] Manycore Tech Inc. SpatialVerse Research Team. Interiors: A 3d gaussian splatting dataset of semantically labeled indoor scenes. <https://huggingface.co/datasets/spatialverse/InteriorGS>, 2025.
- [68] Angel Chang et al. Matterport3d: Learning from rgb-d data in indoor environments. In *Proc. of Int. Conf. 3D Vis.*, pages 667–676, 2017.
- [69] Haotong Lin, Sili Chen, Jun Hao Liew, Donny Y. Chen, Zhenyu Li, Guang Shi, Jiashi Feng, and Bingyi Kang. Depth anything 3: Recovering the visual space from any views. *arXiv preprint arXiv:2511.10647*, 2025.
- [70] Yicong Hong, Zun Wang, Qi Wu, and Stephen Gould. Bridging the gap between learning in discrete and continuous environments for vision-and-language navigation. In *Proceedings of the IEEE/CVF Conference on Computer Vision and Pattern Recognition*, pages 15439–15449, 2022.
- [71] Jiaqi Chen, Bingqian Lin, Xinmin Liu, Xiaodan Liang, and Kwan-Yee K Wong. Affordances-oriented planning using foundation models for continuous vision-language navigation. *arXiv preprint*, 2024.
- [72] Dong An, Zun Wang, Yangguang Li, Yi Wang, Yicong Hong, Yan Huang, Liang Wang, and Jing Shao. 1st place solutions for rxr-habitat vision-and-language navigation competition (cvpr 2022). *arXiv preprint arXiv:2206.11610*, 2022.
- [73] Dong An, Hanqing Wang, Wenguan Wang, Zun Wang, Yan Huang, Keji He, and Liang Wang. Etpnav: Evolving topological planning for vision-language navigation in continuous environments. *IEEE TPAMI*, 2024.
- [74] Zihan Wang, Xiangyang Li, Jiahao Yang, Yeqi Liu, Junjie Hu, Ming Jiang, and Shuqiang Jiang. Lookahead explo-

- ration with neural radiance representation for continuous vision-language navigation. In *CVPR*, 2024.
- [75] Peter Anderson et al. Vision-and-language navigation: Interpreting visually-grounded navigation instructions in real environments. In *Proc. of IEEE/CVF Conf. Comput. Vis. Pattern Recognit.*, pages 3674–3683, 2018.
- [76] John Schulman, Filip Wolski, Prafulla Dhariwal, Alec Radford, and Oleg Klimov. Proximal policy optimization algorithms, 2017.
- [77] Scott Fujimoto, Edoardo Conti, Mohammad Ghavamzadeh, and Joelle Pineau. Benchmarking batch deep reinforcement learning algorithms, 2019.
- [78] Hao Sun, Ziping Xu, Meng Fang, Zhenghao Peng, Jiadong Guo, Bo Dai, and Bolei Zhou. Safe exploration by solving early terminated mdp, 2021.
- [79] Ilya Kostrikov, Ashvin Nair, and Sergey Levine. Offline reinforcement learning with implicit q-learning. In *International Conference on Learning Representations*, 2022.
- [80] Scott Fujimoto and Shixiang Shane Gu. A minimalist approach to offline reinforcement learning, 2021.
- [81] Michael Bain and Claude Sammut. A framework for behavioural cloning. In *Machine Intelligence 15*, 1995.
- [82] Jonathan Ho and Stefano Ermon. Generative adversarial imitation learning, 2016.
- [83] Erik Wijmans, Abhishek Kadian, Ari Morcos, Stefan Lee, Irfan Essa, Devi Parikh, Manolis Savva, and Dhruv Batra. Dd-ppo: Learning near-perfect pointgoal navigators from 2.5 billion frames. *arXiv preprint arXiv:1911.00357*, 2019.
- [84] Fan Yang, Chen Wang, Cesar Cadena, and Marco Hutter. iplanner: Imperative path planning. *arXiv preprint arXiv:2302.11434*, 2023.
- [85] Pascal Roth, Julian Nubert, Fan Yang, Mayank Mittal, and Marco Hutter. Viplanner: Visual semantic imperative learning for local navigation. In *2024 IEEE International Conference on Robotics and Automation (ICRA)*, pages 5243–5249. IEEE, 2024.
- [86] Jiaqi Peng, Wenzhe Cai, Yuqiang Yang, Tai Wang, Yuan Shen, and Jiangmiao Pang. Logoplanner: Localization grounded navigation policy with metric-aware visual geometry. *arXiv preprint arXiv:2512.19629*, 2025.